

# An Investigation on the Interface in a NiTi Short-Fiber-Reinforced 6061 Aluminum Composite by Transmission Electron Microscope

YI LIU, BASEM AL-MATAR, and GOLAM NEWAZ

It has already been demonstrated that NiTi shape-memory alloy fiber-reinforced composites show enhanced mechanical properties by adding a compressive stress to the matrix when the shape-memory effect is activated. The bonding quality between NiTi fiber and the matrix directly affects the stress transfer across the interface, through which the novel functionality of the smart composite is achieved. In the present study, the interface in a NiTi short-fiber-reinforced 6061 aluminum matrix has been investigated by transmission electron microscopy and energy dispersive spectroscopy. Three layers at the interface between NiTi fiber and 6061 aluminum alloy matrix have been found and characterized, *i.e.*, Al<sub>3</sub>Ti with DO<sub>22</sub> ordered structure near the NiTi fiber, Al<sub>9</sub>FeNi with Al<sub>9</sub>Co<sub>2</sub> (or Al<sub>9</sub>Fe<sub>2</sub>) type ordered structure near the Al alloy matrix, and Mg-O layer with 20 nm in thickness between Al<sub>3</sub>Ti and Al<sub>9</sub>FeNi layers. The potential effects of these layers on the mechanical properties of the composite are discussed. Evidence indicates that extensive diffusion from both NiTi fiber and Al alloy matrix occurred during the fabrication of the composite at 570 °C to 580 °C within 20 to 30 minutes. The minor elements in the matrix could be the major elements at the interface. By selecting the chemical composition of the Al alloy matrix, it is possible to control the chemical composition at the interface and further control the mechanical properties of the composites.

DOI: 10.1007/s11661-008-9627-x

© The Minerals, Metals & Materials Society and ASM International 2008

## I. INTRODUCTION

SHAPE-MEMORY alloys (SMA), *e.g.*, NiTi alloy, have been widely used in aerospace,<sup>[1]</sup> biomedical,<sup>[2,3]</sup> and micro-electro-mechanical system<sup>[4-6]</sup> fields, among others. The unique properties of SMA, such as the shape-memory effect, superelasticity, high damping capacity, and bio-compatibility, make it very useful in these fields. One example is to make composites by mixing SMA fibers or particles with other materials, such as metal powders<sup>[7-10]</sup> and polymers,<sup>[11-15]</sup> so that SMA fibers or particles are embedded in the matrix. The composite is usually deformed by either tension or cold rolling at a temperature lower than the starting point of the martensite transformation ( $M_s$ ). Upon heating the composite to the temperature above austenization ( $A_s$ ) of SMA, phase transformation from martensite to austenite will occur. In this process, the SMA will

shrink due to shape recovery and will apply an extra internal compressive stress to the matrix.<sup>[8,16]</sup> When the composite is used in an application, the pre-existing internal compressive stress will compensate the tensile stress applied from the external load, thus improving the tensile and fatigue resistance of the composite. This concept has been confirmed by many experiments.

Furuya<sup>[8]</sup> reported that a 3 vol pct NiTi fiber-reinforced pure Al matrix composite exhibited an increased strength with increasing testing temperature from 20 °C to 100 °C, and the sample with prestrain up to 1.5 pct had higher strength. In addition, the crack propagation rate of the composite was lower at 90 °C than that at room temperature. These results clearly indicate that the compressive stress generated by NiTi SMA at high temperature is beneficial to both the tensile strength and the fatigue life of the composite. Hamada *et al.*<sup>[17]</sup> found that the volume fraction of the NiTi SMA fiber, prestrain, and the history of heat treatment of SMA are the key parameters that affect the yield stress of the NiTi fiber-reinforced 6061 Al alloy composite. Shimamoto *et al.*<sup>[18]</sup> got similar results on fatigue properties in NiTi fiber-reinforced epoxy composites. They found that the resistance of fatigue crack propagation is mainly due to the compressive stress in the matrix caused by the NiTi reverse martensite transformation above  $A_f$ .<sup>[18]</sup> Xie *et al.*<sup>[19]</sup> found that increasing the prestrain will increase the yield stress of the NiTi short-fiber-reinforced 6061 Al composite, increasing the temperature will increase the strengthening effect, whereas increasing the ratio of the axis/diameter of the fiber to above 5 will not increase

---

YI LIU, Research Associate and Manager, is with the Laboratory of Analytical Electron Microscopy, Central Instrument Facility, Department of Chemistry, Wayne State University, Detroit, MI 48202. Contact e-mail: yliu@chem.wayne.edu BASEM AL-MATAR, formerly Ph.D. Student, Department of Mechanical Engineering and Institute for Manufacturing Research, Wayne State University, is Senior Design Engineer, Baker Oil Tools, Houston, TX 77019. GOLAM NEWAZ, Professor, is with the Department of Mechanical Engineering and Institute for Manufacturing Research, Wayne State University.

Manuscript submitted April 9, 2007.

Article published online September 11, 2008

the yield stress of the composite. Port *et al.*<sup>[16,20]</sup> studied fatigue and fracture behavior of a 10 vol pct NiTi particle-reinforced Al composite fabricated by a powder metallurgy process. The NiTi particles of 5  $\mu\text{m}$  in diameter were obtained by mechanically milling particles of 40  $\mu\text{m}$  in diameter.<sup>[21]</sup> The composite was cold rolled at  $-30\text{ }^\circ\text{C}$  in order to activate the shape-memory effect when the samples were tested at the temperature above  $A_s$ . Port *et al.*<sup>[20]</sup> found that a smaller NiTi particle size of 5  $\mu\text{m}$  provides a higher strengthening effect than that provided by a NiTi particle size of 40  $\mu\text{m}$ ; and mechanically milled particles provide further strengthening than the particles without mechanical milling. The yield stress and ultimate strength were found to increase about 43 and 54 pct, respectively. However, at the same time, the elongation was found to decrease, which is normal for almost all composites.

There is no doubt that the interface between the NiTi fiber/particle and the matrix should be bonded very well to ensure the continuity of stress and strain. Further, the interface not only transfers stress from NiTi SMA to the matrix, it is a potential source of cracks as well. Therefore, studies on the interface are very important. However, up to now, studies focusing on the interface in NiTi SMA-reinforced Al composites are very limited, and only a few studies are documented in the literature. By using scanning electron microscopy (SEM) and energy dispersive spectroscopy (EDS), Hamada *et al.*<sup>[17]</sup> found that diffusion occurred from both the NiTi fiber and the 6061 Al matrix due to hot pressing during the fabrication of the composite. They estimated from the EDS analyses that, in the sample hot pressed at  $500\text{ }^\circ\text{C}$ , the interface phase might be  $\text{Al}_3\text{Ti}$ , while in the samples hot pressed at  $550\text{ }^\circ\text{C}$  and  $600\text{ }^\circ\text{C}$ , the interface phases might be  $\text{Al}_3\text{Ti}$  and  $\text{Al}_3\text{Ni}$ . Because both  $\text{Al}_3\text{Ti}$  and  $\text{Al}_3\text{Ni}$  are intermetallics and brittle, cracks would form at the interface easily and reduce the continuity of the stress/strain between the NiTi fiber/particle and the matrix.<sup>[17]</sup> In another study on NiTi/Al6061 SMA composite,<sup>[22]</sup> the authors showed a 4- $\mu\text{m}$  diffusion layer with low contents of Al, Ti, and Ni but high content of Mg and Si by SEM and electron probe microanalysis (EPMA). However, the authors did not further discuss the interface. Mizuuchi *et al.*<sup>[23]</sup> studied the interface chemistry in a NiTi fiber-reinforced AZ31 Mg alloy by SEM and EDS. The EDS elemental mapping analysis shows two phases existing at the interface. The phase near the matrix is a 2- $\mu\text{m}$ -thick layer consisting of Al and Ni, while the other phase next to the matrix is a 10- $\mu\text{m}$  layer in thickness with Mg, Al, and oxygen. However, due to the limited resolution of SEM, there is no clear picture of the interface, and there is no information about the crystal structure of the phases formed at the interface. Therefore, it is hard to confirm the phases formed at the interface only based on SEM and EDS. Up to now, to our knowledge, there is no analysis *via* transmission electron microscopy (TEM) on the interface between the NiTi fiber and Al matrix reported in the literature.

Because the interface between the NiTi fiber/particle and Al matrix is a critical factor for the enhancement in

mechanical properties of the SMA-reinforced composite, and is related to diffusion and phase formation, it is necessary to characterize it in detail so that the function of the interface can be better understood and controlled. In the present study, investigations by TEM and EDS on the interface between the NiTi fiber and 6061 Al matrix will be presented.

## II. EXPERIMENTAL DETAILS

The NiTi short-fiber-reinforced 6061 Al composite was fabricated using a pressure-assisted sintering process in ambient air, as described in the previous article by Xie *et al.*<sup>[19]</sup> The NiTi short fiber was purchased from Nitinol Devices & Components (Fremont, CA), and the 6061 Al powders were purchased from Valimet Inc., Stockton, CA. The nominal chemical composition of NiTi fiber is Ni54.5, oxygen  $\leq 0.05$ , carbon  $\leq 0.02$ , and balance Ti (wt pct), while the chemical composition of 6061 Al powder is Cr0.08, Cu0.27, Fe0.26, Mg0.97, Mn0.02, Si0.56, Ti0.02, Zn0.05, and balance Al (wt pct). Based on the measurement by differential scanning calorimetry in the previous article,<sup>[19]</sup> the martensite transformation of NiTi fiber ready for making the composite starts at  $45.7\text{ }^\circ\text{C}$  ( $M_s$ ) and finishes at  $37.3\text{ }^\circ\text{C}$  ( $M_f$ ). A 5 pct volume fraction of NiTi short fibers with 300  $\mu\text{m}$  in diameter was mixed with 6061 Al powder with 30  $\mu\text{m}$  in diameter in a mold. The NiTi fibers were prealigned. Sintering of the 6061 Al alloy powders and the NiTi fibers was conducted in two steps: first, the premix was compressed at a uniaxial stress of 70 MPa at room temperature, and then the mold containing the premix was sintered at high temperature under pressure. It was found that four factors are critical: heating rate, sintering temperature, pressure, and time. Good sintering quality of the composite, which was reflected by mechanical property tests, was obtained at a heating rate of  $20\text{ }^\circ\text{C}/\text{min}$ , a sintering temperature of  $570\text{ }^\circ\text{C}$  to  $580\text{ }^\circ\text{C}$ , and a hot uniaxial pressure of 50 to 70 MPa perpendicular to the prealigned fibers for 20 to 30 minutes.<sup>[19]</sup> The sintering process was finished by using induction heating coil set up on a MTS 801 test system (Eden Prairie, MN), and the maximum load was 220 kN.

The TEM foils were sliced from the as-prepared composite along the cross-sectional direction, which is perpendicular to the long axis of the NiTi fiber. The slices were then mechanically thinned by using sand paper from 300 grit down to 2400 grit. In order to locate the interface of the NiTi fibers with the Al matrix, the sample was dimple grinded and polished on a dimpling grinder (Fischione, model 200, Export, PA). Final thinning was completed by ion-beam milling using a Gatan 691 precision ion polishing system (Pleasanton, CA). The voltage was 4.5 kV and the polishing angle was 5 deg. The polishing was stopped when a hole appeared and extended to the interface between the NiTi fiber and matrix, which was easily found because the NiTi fiber is large in dimension.

The SEM observations were conducted on a Hitachi 2400 scanning electron microscope (Tokyo, Japan) operating at 25 kV. The sample for SEM observations

was mechanically polished and etched by Keller's agent. The TEM observations were conducted on a JEOL\*

---

\*JEOL is a trademark of Japan Electron Optics Ltd., Tokyo.

---

2010 FasTEM high-resolution transmission electron microscope equipped with an EDS system (EDAX Inc., Mahwah, NJ) operating at 200 kV. A double tilt sample holder was used to obtain diffraction patterns from the interface area. Selected area electron diffraction patterns are analyzed with the aid of "jems" software, which is developed by Professor P. Stadelmann (CIME, EPFL, Lausanne, Switzerland) and is based on the widely accepted theory of electron diffraction of thin crystals.<sup>[24]</sup>

### III. EXPERIMENTAL RESULTS

Figure 1 shows a typical microstructure of a NiTi fiber-reinforced 6061 Al composite observed by SEM. The dimension of the NiTi fiber is 300  $\mu\text{m}$ . The average intercept length of the grains in the 6061 Al matrix was measured to be 8.2  $\mu\text{m}$ , which corresponds to an average grain size of 14.3  $\mu\text{m}$ . Figure 2(a) shows a TEM bright-field image of an interface in the NiTi fiber-reinforced 6061 Al composite. Because the dimension of the NiTi fiber is very large, and the thinning rate of the NiTi fiber is different from that of the Al matrix, to make the NiTi fiber and the Al matrix be transparent to the electron beam at the same time is difficult. Two obvious layers can be found at the interface between the NiTi fiber and 6061 Al matrix. The EDS analyses indicate that the two layers have different chemical compositions. The layer that is close to the NiTi fiber and is denoted as "Ti-Al" in Figure 2(a) contains Ti, Al, some Si, and a small amount of Ni, while the layer that is close to the 6061 Al matrix and is denoted as

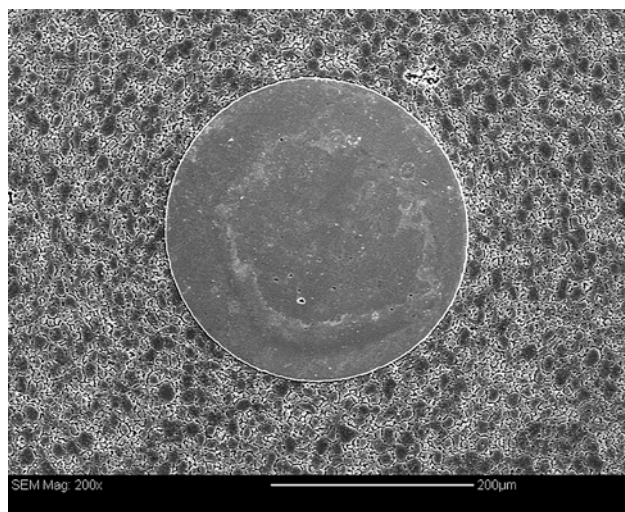


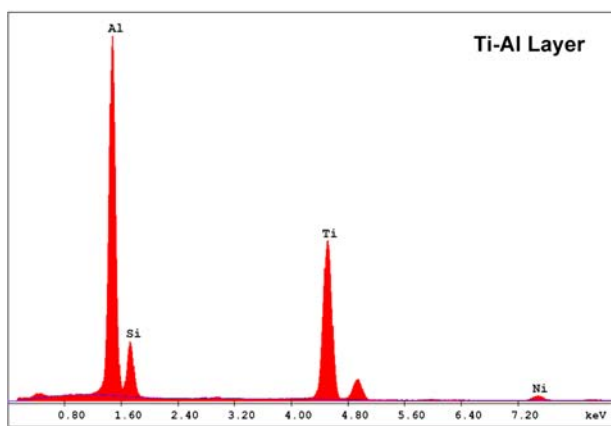
Fig. 1—Typical microstructure of NiTi short-fiber-reinforced 6061 Al composite. The dimension of NiTi fiber is about 300  $\mu\text{m}$ , and the grain size of 6061 Al in the matrix is 14.3  $\mu\text{m}$ .

"Al-Fe-Ni" in Figure 2(a) contains Al, Ni, Fe, Si, and a small amount of Ti. Based on at least six measurements of the chemical composition on the two layers shown in Figure 2(a), the average chemical compositions of the two layers are given in Table I. Typical EDS spectra collected from the two layers are shown in Figures 2(b) and (c), respectively. The maximum thicknesses of the Ti-Al and Al-Fe-Ni layers are about 1.5 and 1  $\mu\text{m}$ , respectively, resulting in the total thickness of the multilayers of 2.5  $\mu\text{m}$ . The EDS analyses indicate that extensive diffusion from both the NiTi fiber and 6061 Al matrix occurred during the bonding process, *i.e.*, Ti and Ni diffused from the NiTi fiber, and Al, Fe, and Si diffused from the 6061 Al matrix. Because there are only Ni, Ti, and a small amount of O in the NiTi fibers, it is interesting to find Fe element in the second layer Al-Ni-Fe, because the Fe content in the current 6061 Al powders is only 0.26 in weight percent<sup>[19]</sup> while it is 17.4 in weight percent in the Al-Fe-Ni layer found in the present study. Probably the small amount of Fe is very easily absorbed by Ni. By diffusion of the elements from both the NiTi fiber and 6061 Al matrix, the layers on the interface formed.

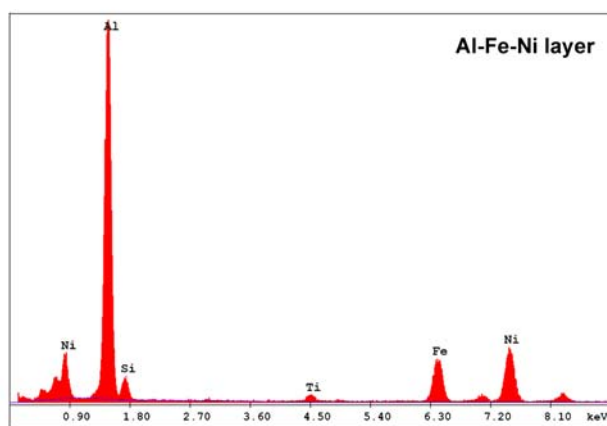
As listed in Table I, the Ti-Al layer contains Al57.6, Ti30.2, and Si11.2 (at. pct). Based on the Ti-Al binary alloy phase diagram<sup>[25]</sup> and the Ti-Al-Si ternary phase diagram,<sup>[26]</sup> the most likely intermetallic compound formed in this layer is either  $\text{Al}_3\text{Ti}$ , which has  $\text{DO}_{22}$  ordered crystal structure, or  $\text{TiAl}$ , which has  $\text{L1}_0$  ordered crystal structure. Silicon can be dissolved into both  $\text{Al}_3\text{Ti}$  and  $\text{TiAl}$  up to a certain amount. The  $\text{DO}_{22}$   $\text{Al}_3\text{Ti}$  is an ordered tetragonal structure, as shown in Figure 3(a), and its lattice parameters are  $a = b = 0.384$  nm,  $c = 0.8579$  nm, with  $c/a = 2.234$ , while the  $\text{L1}_0$   $\text{TiAl}$  is a near-cubic ordered tetragonal structure, as shown in Figure 3(b), and its lattice parameters are  $a = b = 0.3997$  nm,  $c = 0.4062$  nm, with  $c/a = 1.02$ .<sup>[27]</sup> Because the electron diffraction patterns usually have multiple solutions, in order to uniquely determine the phase formed at the interface, a series of electron diffraction patterns from selected areas of the Ti-Al layer were obtained and some of the representative patterns are shown in Figure 4. All the diffraction patterns shown in Figure 4 could be indexed as the  $\text{DO}_{22}$  ordered structure, while some of the patterns could also be indexed as  $\text{L1}_0$  ordered structure, suggesting that the Ti-Al layer is  $\text{Al}_3\text{Ti}$ , as estimated in the study on interface between NiTi fiber and Al matrix by Hamada *et al.*<sup>[17]</sup> The entire indexing process was assisted and confirmed by the simulation software jems, and some of the simulated diffraction patterns of  $\text{Al}_3\text{Ti}$  are shown in Figure 5. Space group, atom positions, and lattice parameters of the possible phases are needed to perform the simulations. It can be seen that the simulated diffraction patterns (Figure 5) are consistent with those obtained from experiment (Figure 4). After careful calibration of the camera length by using the polycrystalline Al standard sample, the lattice parameters of the  $\text{Al}_3\text{Ti}$  layer have been estimated to be  $a = 0.386$  nm and  $c = 0.822$  nm, which is very close to the lattice parameter of the  $\text{Al}_3\text{Ti}$  intermetallic compound reported in the literature.<sup>[27,28]</sup> It is noticed that



(a)



(b)



(c)

Fig. 2—(a) TEM bright-field image showing the multilayers formed at the interface between the NiTi short fiber and 6061 Al matrix, and typical EDS spectra corresponding to the (b) Ti-Al layer and (c) Al-Fe-Ni layer.

**Table I. Typical Average Chemical Compositions in Ti-Al and Al-Fe-Ni Layers Detected by EDS**

Elements Percentage	Al		Ti		Ni		Fe		Si	
	At. Pct	Wt Pct	At. Pct	Wt Pct	At. Pct	Wt Pct	At. Pct	Wt Pct	At. Pct	Wt Pct
Ti-Al layer	57.6	44.8	30.2	42.9	0.95	1.7	NA*	NA	11.2	9.4
Al-Fe-Ni layer	70.3	55.4	1.3	1.8	12.2	20.9	10.7	17.4	5.5	4.5

\*NA = not applicable.

the Ti-Al layer contains 11.2 at. pct Si (or 9.4 wt pct). According to the Ti-Al-Si ternary diagram,<sup>[26]</sup> Al<sub>3</sub>Ti can dissolve a certain amount of Si. Further, the fact that Si can be dissolved into Al<sub>3</sub>Ti up to 11.59 wt pct has been reported.<sup>[29]</sup> No Ti-Si compounds have been detected in our experiments based on the diffraction patterns obtained from the Ti-Al layer.

Electron diffraction patterns from selected areas of Al-Ni-Fe layer were also recorded, as shown in Figure 6. It was reported by Hamada *et al.*<sup>[17]</sup> that, in addition to Al<sub>3</sub>Ti, another layer of Al<sub>3</sub>Ni could form at the interface

between NiTi fiber and 6061 Al matrix in NiTi fiber-reinforced 6061 Al composite. However, because the conclusion was only based on the EDS experiments, and there were no diffraction patterns, the formation of Al<sub>3</sub>Ni on the interface was not conclusive. Al<sub>3</sub>Ni has a DO<sub>20</sub> ordered structure, which is an ordered orthorhombic crystal structure with  $a = 6.5982$  nm,  $b = 7.3515$  nm, and  $c = 4.8021$  nm.<sup>[27]</sup> From the diffraction patterns shown in Figure 6(a) obtained in the present study, the crystal structure of the Al-Fe-Ni layer should be very close to a tetragonal structure, because

the diffraction pattern shows nearly fourfold symmetry. This excludes the possibility that the Al-Fe-Ni layer is  $\text{Al}_3\text{Ni}$ . Except for the pattern shown in Figures 6(c) and (h), all the diffraction patterns shown in Figure 6 are

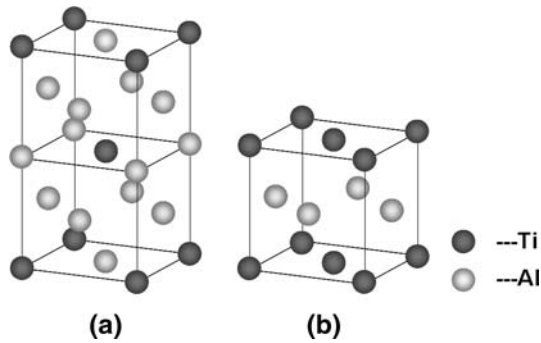


Fig. 3—Schematic atom arrangement of (a)  $\text{Al}_3\text{Ti}$  with  $\text{DO}_{22}$  ordered structure and (b)  $\text{TiAl}$  with  $\text{L1}_0$  ordered structure.

typical patterns of a fcc structure. Considering the patterns to be from an fcc structure, the lattice parameter was calculated as  $a = 0.9035 \text{ nm}$ . This is very close to  $\text{FeNiAl}_2$ , which has  $\text{BiF}_3$  (or  $\text{CsCl}$ ) ordered structure (fcc) with lattice parameter  $a = 1.0614 \text{ nm}$ .<sup>[30]</sup> Some articles classify this structure as  $\text{L2}_1$ , which actually contains eight  $\text{CsCl}$  cells.<sup>[31]</sup> However, the diffraction pattern shown in Figures 6(c) and (h) could not be assigned to  $\text{FeNiAl}_2$ , and there is an angle of  $86^\circ$  between the two crystal axes marked in Figure 6(h) that should be  $90^\circ$  if the compound has cubic structure, implying that the phase belongs to a crystal system, which is not orthogonal (including cubic and tetragonal), but rather a monoclinic structure.

It has been reported that<sup>[32]</sup> the  $\text{Al}_9\text{FeNi}$  phase contains Fe 4.5 to 14 and Ni 18 to 28 (wt pct). As listed in Table I, the Al-Fe-Ni layer contains Fe17.4 and Ni20.9 (wt pct). So the chemical composition of the Al-Fe-Ni layer found in the present study is very close to that of  $\text{Al}_9\text{FeNi}$ , which has a monoclinic crystal structure similar to  $\text{Al}_9\text{Co}_2$  (or  $\text{Al}_9\text{Fe}_2$ ) and has a space group

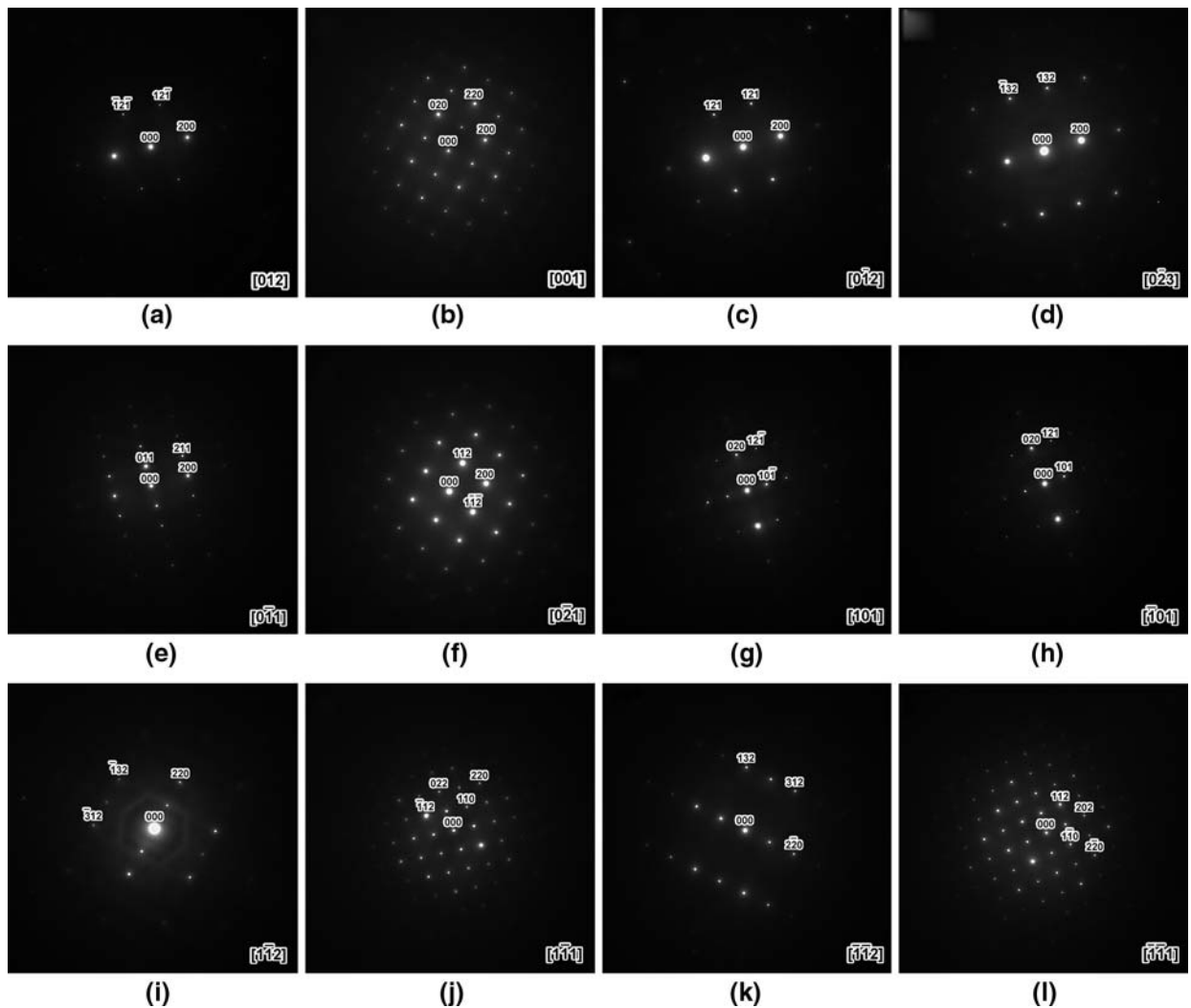


Fig. 4—Diffraction patterns from the selected area in Ti-Al layer of the interface between NiTi fiber and 6061 Al matrix. The patterns are indexed as  $\text{DO}_{22}$   $\text{Al}_3\text{Ti}$  with the orientations (a)  $[012]$ , (b)  $[001]$ , (c)  $[012]$ , (d)  $[023]$ , (e)  $[011]$ , (f)  $[021]$ , (g)  $[101]$ , (h)  $[\bar{1}01]$ , (i)  $[112]$ , (j)  $[111]$ , (k)  $[\bar{1}\bar{1}2]$ , and (l)  $[\bar{1}\bar{1}1]$ .

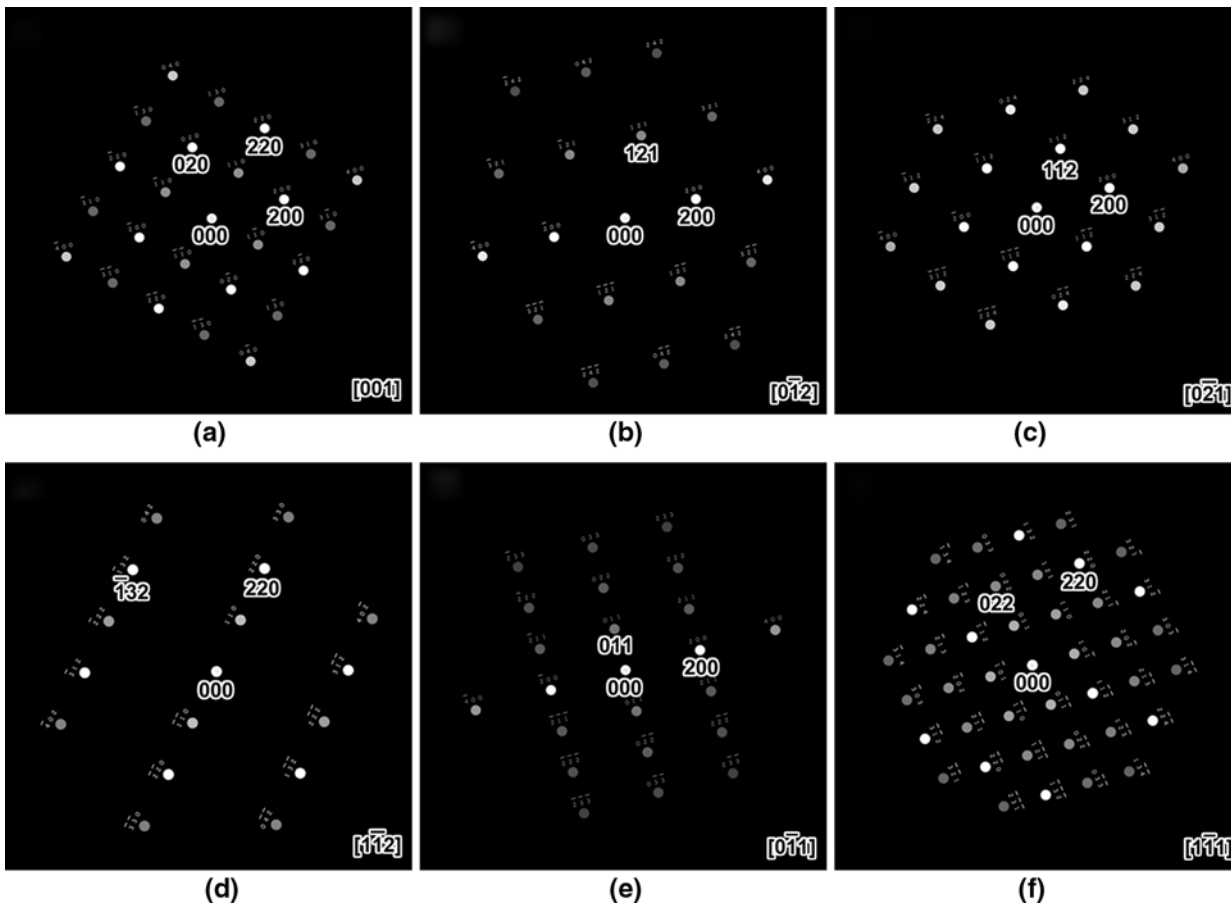


Fig. 5—Simulated diffraction patterns of DO<sub>22</sub> Al<sub>3</sub>Ti with the foil normal parallel to (a) [001], (b) [0 $\bar{1}$ 2], (c) [0 $\bar{2}$ 1], (d) [1 $\bar{1}$ 2], (e) [0 $\bar{1}$ 1], and (f) [1 $\bar{1}$ 1].

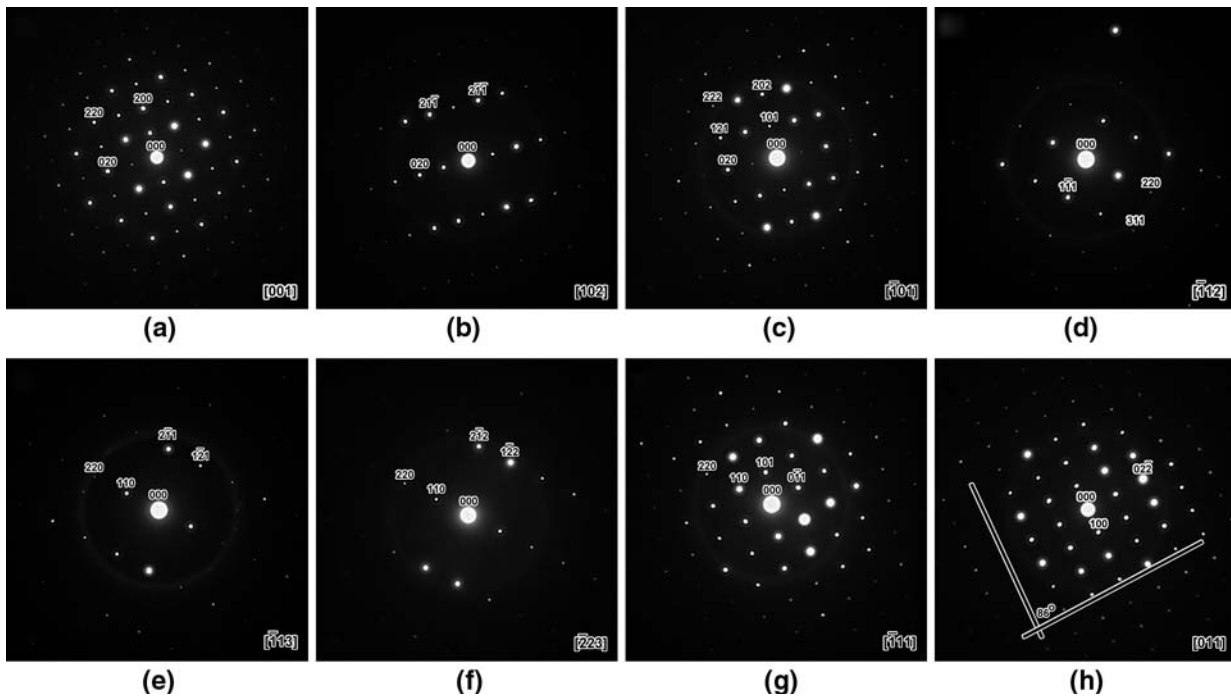


Fig. 6—Diffraction patterns from the selected area in Al-Fe-Ni layer of the interface between NiTi fiber and 6061 Al matrix. The patterns are indexed as Al<sub>6</sub>FeNi with the orientations (a) [001], (b) [102], (c) [101], (d) [112], (e) [113], (f) [223], (g) [111], and (h) [011].

$P2_1/c$ .<sup>[27,33]</sup> The lattice parameters of  $Al_9FeNi$  are  $a = 0.6207$  nm,  $b = 0.6271$  nm,  $c = 0.8598$  nm, and  $\beta = 94.66$  deg,<sup>[34]</sup> while the lattice parameters of  $Al_9Co_2$  are  $a = 0.6213$  nm,  $b = 0.6290$  nm,  $c = 0.85565$  nm, and  $\beta = 94.76$  deg.<sup>[27]</sup> So they are very close. All the diffraction patterns obtained from the Al-Fe-Ni layer could be indexed as  $Al_9Fe_2$ , as shown in Figure 6. Based on the indexed diffraction patterns and the calibrated camera length, and supposing  $\beta = 94.66$  deg, the lattice parameters of the Al-Fe-Ni phase were calculated as  $a = 0.634$  nm,  $b = 0.633$  nm, and  $c = 0.883$  nm, which is close to the reported data.<sup>[34]</sup> More accurate calculations are possible based on more accurate measurements, but for the purpose of checking the possible structure, it is good enough. All the indexing was assisted and confirmed by using the jems software, and some of the supportive information is shown in Figure 7. Again, it can be seen that the simulated patterns (Figure 7) are consistent with those obtained by experiment (Figure 6). The occupation of Al and Fe (or Co) in  $Al_9Fe_2$  ( $Al_9Co_2$ ) can be found in Reference 27. Figure 8 schematically shows the lattice arrangement of  $Al_9Fe_2$ .

Figure 9 shows dislocations (Figure 9(a)) and a stacking fault (Figure 9(b)) found in the  $Al_3Ti$  layer formed at the interface between the NiTi fiber and the 6061 Al matrix. It is interesting to find that locally the

$Al_3Ti$  layer can be deformed, as shown in the areas labeled as A and B in Figure 9(a). Dislocations and stacking faults are two common deformation features in the  $Al_3Ti$  phase. The deformation structure could result from the hot-pressing process during the fabrication of the composite.

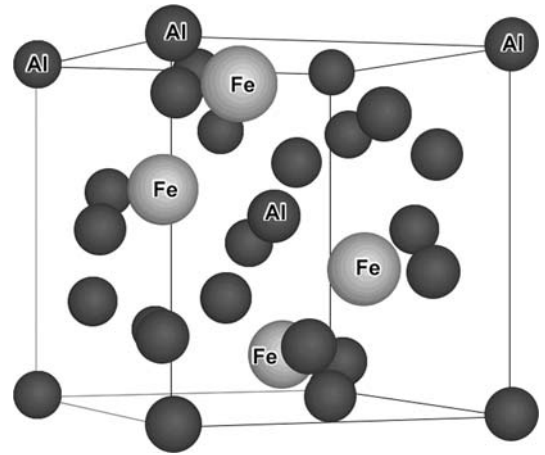


Fig. 8—Atom occupations in  $Al_9Fe_2$  phase generated by jems software by inputting the atom positions reported in Ref. 27.

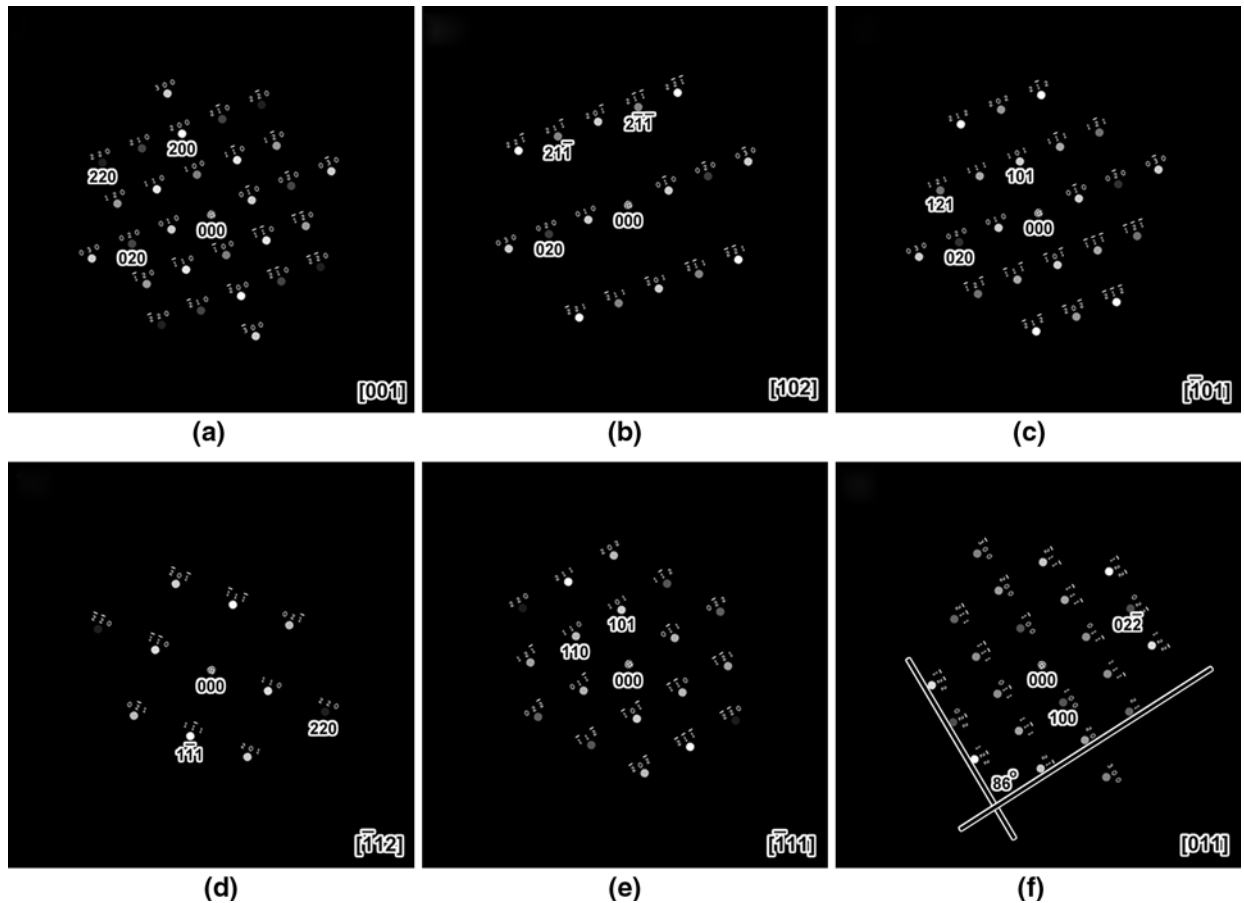


Fig. 7—Simulated diffraction patterns of  $Al_9Fe_2$  ordered structure with the foil normal parallel to (a)  $[001]$ , (b)  $[102]$ , (c)  $[\bar{1}01]$ , (d)  $[\bar{1}12]$ , (e)  $[\bar{1}11]$ , and (f)  $[011]$ .

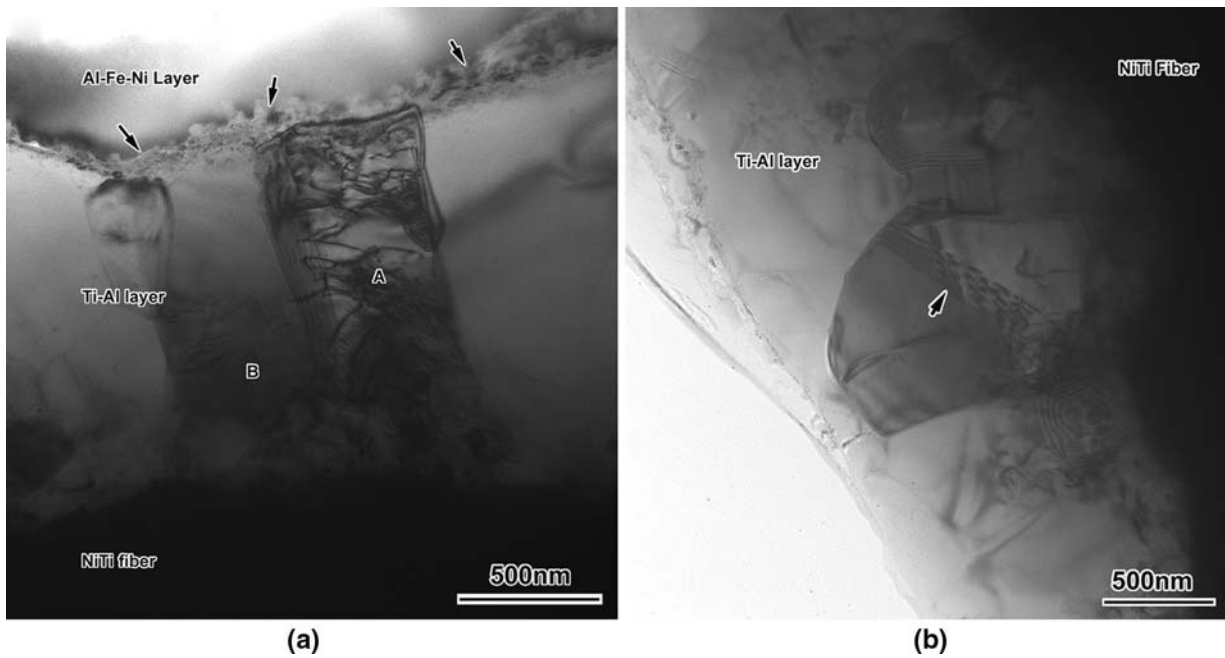


Fig. 9—(a) Dislocations and (b) a stacking fault found the  $\text{Al}_3\text{Ti}$  layer formed at the interface between the NiTi fiber and 6061 Al matrix.

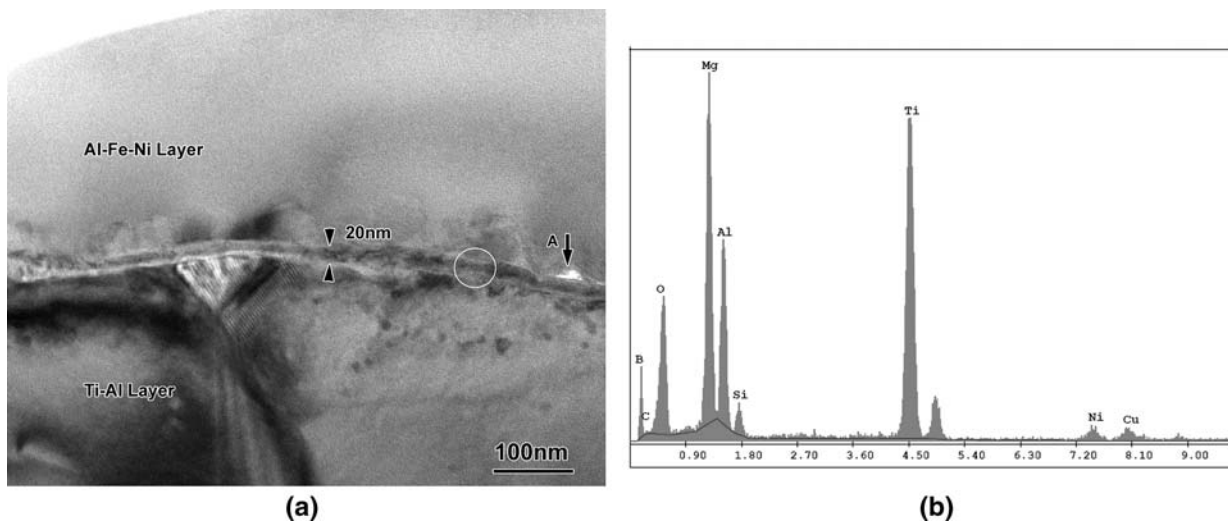


Fig. 10—(a) Mg-O thin layer with 20 nm in thickness between  $\text{Al}_3\text{Ti}$  and  $\text{Al}_9\text{FeNi}$  layers and (b) EDS spectrum obtained from the circled area.

Table II. Typical Chemical Composition in Mg-O-Al Layer

Elements	Mg (At. Pct)	Al (At. Pct)	O (At. Pct)	Ti (At. Pct)	Si (At. Pct)	Ni (At. Pct)
Content	26.0	12.4	31.4	27.0	2.0	1.2

It can be found from Figure 9(a) that, at the boundary between the  $\text{Al}_3\text{Ti}$  and  $\text{Al}_9\text{FeNi}$  phases, there exist areas with different contrast, as indicated by the arrows. Further TEM observations and EDS analyses indicate that there is another layer of about 20 nm in thickness between the  $\text{Al}_3\text{Ti}$  and  $\text{Al}_9\text{FeNi}$  layers (Figure 10(a)). This thin layer contains excessively high percentages of Mg and oxygen, as shown in

Figure 10(b), which were not found in either the NiTi fiber or the 6061 Al matrix. For convenience, we call this layer the Mg-O layer. A typical chemical composition of this layer shown in Figure 10 is listed in Table II, and both Ti and Al were detected. Because the beam size is larger than the thickness of the Mg-O layer, at least part of the percentage of Ti and Al is contributed from the  $\text{Al}_3\text{Ti}$  and  $\text{Al}_9\text{FeNi}$  layers in addition to the Mg-O layer



itself. The most likely phases formed here could be any product between Mg, O, Al, Ti, Fe, or Ni, such as the spinel phase ( $\text{MgAl}_2\text{O}_4$ ) or  $\text{MgO}$ , which are ceramics phases and are brittle. Because this layer is not continuous, and sometimes voids could be found in this layer, as indicated by arrow "A" in Figure 10(a), this layer will not be good for the overall bonding between the NiTi fiber and Al matrix and thus is unfavored. Because the 6061 Al alloy used in the present study contains 0.97 wt pct Mg,<sup>[19]</sup> the Mg existing at the interface diffused from the 6061 Al matrix.

Observations along the interface between the NiTi fiber and the 6061 Al matrix showed that the  $\text{Al}_9\text{FeNi}$  layer did not form along the entire interface. At the location where there is no  $\text{Al}_9\text{FeNi}$  layer, as shown in Figure 11(a), a high percentage of Mg and O could still be detected at and near the boundary between the  $\text{Al}_3\text{Ti}$  and the 6061 Al matrix, as indicated by EDS analyses in Figures 11(b) and (c). In areas far away from the boundary, neither Mg nor oxygen could be found.

#### IV. DISCUSSION

The quality of bonding between the NiTi fiber and the Al matrix is very important for the enhancement of the mechanical properties of the smart composite, because it directly affects the continuity of the compressive stress transferred to the matrix from the SMA. Although the NiTi fiber-reinforced Al matrix composite has been one of the active fields of materials research for many years since the concept of the compressive stress to the matrix generated by SMA was proposed,<sup>[8]</sup> very few studies focusing on the interface between the NiTi fiber and the matrix were reported in the literature. Hamada *et al.*<sup>[17]</sup> provided the most detailed results, but the results were based only on EDS analyses instead of information about the crystal structure; therefore, the findings were not conclusive. In the present study, using diffraction patterns and EDS analyses obtained from the interface, three layers at the bonding area between the NiTi fiber and the 6061 Al matrix have been clearly identified. Two continuous layers have been confirmed to be  $\text{Al}_3\text{Ti}$  and  $\text{Al}_9\text{FeNi}$  phases, and one thin layer between the two phases contains a high percentage of Mg and oxygen.

Intermetallics, as bulk materials, are usually brittle. However, the thin layer of  $\text{Al}_3\text{Ti}$  found in the present study shows some ductility (Figure 9), which should be beneficial to the composite. If it is too brittle, cracks will be initiated and the stress continuity will be destroyed. However, if the phase formed at the interface is too ductile, it will absorb the stress generated by the SMA and thus weaken the shape-memory effect. Even though there is no experimental evidence, the  $\text{Al}_9\text{FeNi}$  layer appears not to be very ductile, based on the fact that a low dislocation density was found in this layer. Considering the large lattice parameters, the slip vector of the  $\text{Al}_9\text{FeNi}$  phase is very large, which makes the deformation difficult. The thin layer of Mg-O found at the interface between  $\text{Al}_3\text{Ti}$  and  $\text{Al}_9\text{FeNi}$  layers is unfavored, because this layer is brittle and is not continuous,

and it decreases the strength of the phase boundary between  $\text{Al}_3\text{Ti}$  and  $\text{Al}_9\text{FeNi}$ .

The current study on the interface between the NiTi fiber and the 6061 Al matrix clearly indicates that extensive diffusion occurred during the composite preparation at 570 °C to 580 °C with the aid of a pressure between 50 to 70 MPa within 20 to 30 minutes, as described in Section II. More interestingly, from the present study, it is found that the minor elements in the 6061 Al matrix are easy to diffuse and could be the major elements in the layers formed at the interface between the NiTi fiber and the 6061 Al matrix. For example, the 6060 Al matrix contains only Fe0.26, Si0.56, and Mg0.97 (wt pct),<sup>[19]</sup> but they diffused to the bonding area and became the major elements in the newly formed  $\text{Al}_3\text{Ti}$  layer, which contains 9.4 wt pct Si; the  $\text{Al}_9\text{FeNi}$  layer, which contains 17.4 wt pct Fe; and the Mg-O layer between them. Although NiTi fiber contains a small amount of oxygen ( $\leq 0.05$  wt pct), it is more likely that the oxygen in the Mg-O layer between  $\text{Al}_3\text{Ti}$  and  $\text{Al}_9\text{FeNi}$  layers came from 6061 Al powders during the fabrication of the composite. Besides, a high percentage of Mg and O were also found at the area near the boundary between  $\text{Al}_3\text{Ti}$  and 6061 Al matrix, as shown in Figure 11. The behavior of Mg and oxygen indicates that they prefer to segregate at the interface. Therefore, Mg and oxygen are the two elements that need to be avoided or controlled during the preparation of the composite. Other elements, such as Cr, Cu, Mn, and Zn, were not detectable in the bonding area, indicating that they were not actively involved in the diffusion process. Therefore, it should be possible to control the chemistry at the interface by carefully selecting the chemical composition of the matrix, thus controlling the mechanical properties of the composite. More studies are needed in this field.

Although the concept of an SMA-reinforced Al composite has been confirmed by many experiments,<sup>[7-9,11-14,16-23,35]</sup> the present study shows that the current design of the composite is still in need of improvement. The main problem is that the dimensions of the NiTi fibers used in the current studies reported in the literature are too large (190 to 500  $\mu\text{m}$ ) compared with the grain size of the Al matrix (5 to 15  $\mu\text{m}$ ). As a result, the composite usually failed due to the strength mismatch between the NiTi fiber and the Al alloy matrix.<sup>[19]</sup> When the composite is under loading conditions, the fiber will undertake a higher percentage of the load so that the bonding acts as a minor role and cracks usually initiate from the interface. As a result, the "pull out" mechanism of NiTi fibers was frequently observed.<sup>[19]</sup> For the same reason, as indicated previously, the prestrain that is needed to activate the shape-memory effect could not be increased too much, and is usually less than 0.01 in order to avoid failure.<sup>[19]</sup> The quality of bonding would be more important when the dimension of the NiTi fiber is significantly reduced to the same range as the grain size of the matrix. To this point, Port *et al.*<sup>[16,20,21]</sup> had a good beginning by using NiTi SMA particles to reinforce the composite with a minimized dimension of NiTi SMA particles. In their study, NiTi particles of 5  $\mu\text{m}$  in diameter were used to

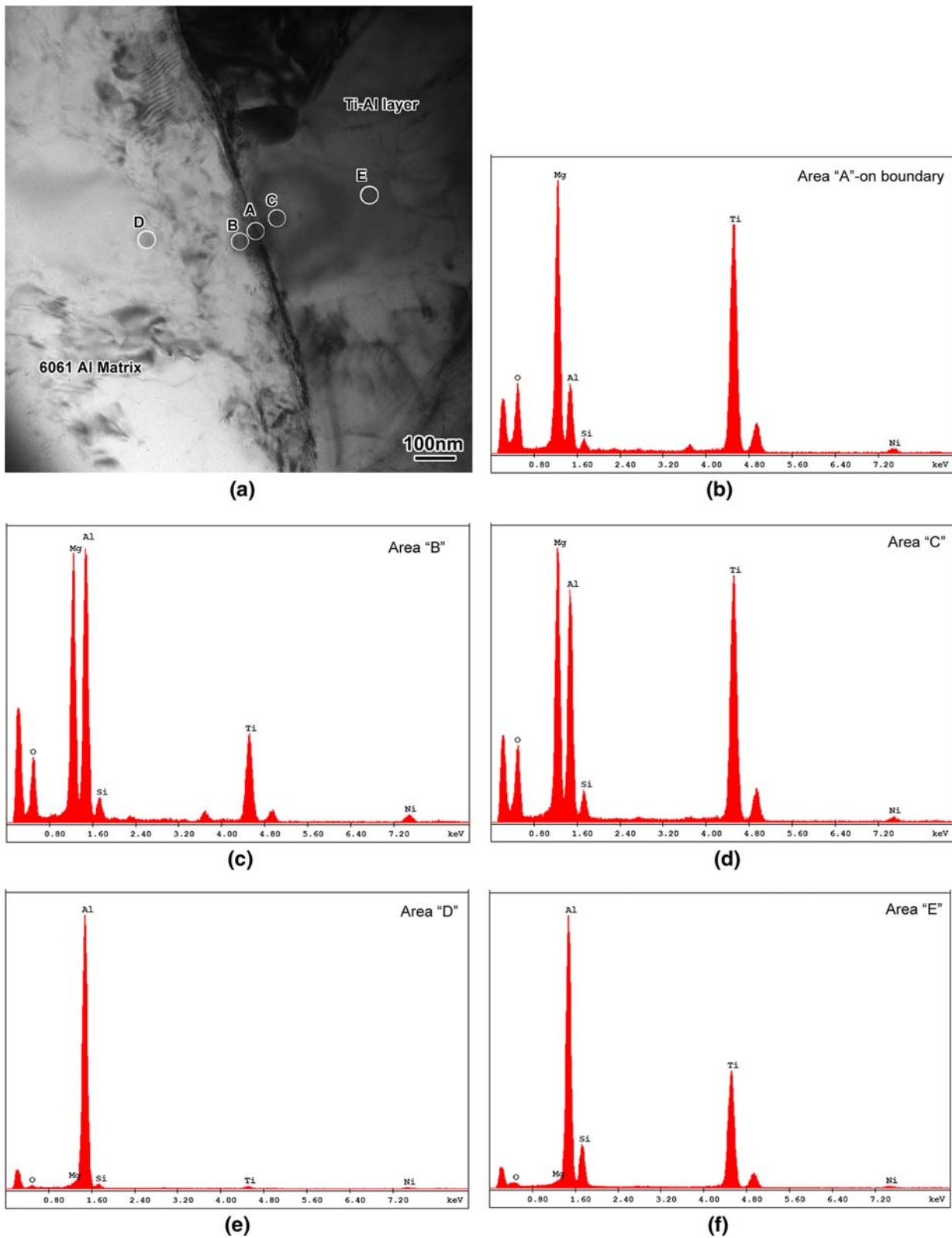


Fig. 11—(a) TEM photo showing the interface between the  $\text{Al}_3\text{Ti}$  layer and 6061 Al matrix without  $\text{Al}_3\text{FeNi}$  layer, and typical EDS analyses on the areas (b) A—boundary, (c) B—near boundary at Al side, (d) C—near boundary in Ti-Al side, (e) D—far away from the boundary on Al side, and (f) E—far away from the boundary in Ti-Al side.

reinforce the Al matrix. They found<sup>[20]</sup> that the smaller NiTi particles provide a higher strengthening effect than that provided by a NiTi particle size of  $40\ \mu\text{m}$ , and the

yield stress and ultimate strength were increased about 43 and 54 pct, respectively, in the  $5\text{-}\mu\text{m}$  NiTi particle-reinforced Al composite.

## V. CONCLUSIONS

The interface in a NiTi short-fiber-reinforced 6061 Al composite has been investigated by TEM and EDS. Three layers have been found at the interface between the NiTi fiber and Al matrix, *i.e.*, Al-rich single-phase Al<sub>3</sub>Ti with a DO<sub>22</sub> ordered structure, Al<sub>9</sub>FeNi (space group P2<sub>1</sub>/c), with Al<sub>9</sub>Co<sub>2</sub> (or Al<sub>9</sub>Fe<sub>2</sub>) type ordered structure, and one discontinuous thin layer of Mg-O of 20 nm in thickness between the Al<sub>3</sub>Ti and Al<sub>9</sub>FeNi layers. The Mg-O layer contains a high percentage of Mg and oxygen and is estimated to be MgO or other products arising from Mg-O and Al, Ti, such as MgAl<sub>2</sub>O<sub>4</sub>. Segregation of Mg and oxygen was also found at the vicinity of the interface between the NiTi fiber and 6061 Al matrix. It is found that the Al<sub>3</sub>Ti layer shows some ductility, while the Al<sub>9</sub>NiFe layer contains a very low dislocation density. Considering that the slip vector of Al<sub>9</sub>NiFe phase is large, deformation would not be favored in the Al<sub>9</sub>NiFe layer. Because the Mg-O layer is not continuous, and sometimes voids could be found, it weakens the strength of the phase boundary between the NiTi SMA and the Al matrix.

Evidence indicates that extensive diffusion from both the NiTi fiber and the Al matrix occurred; *i.e.*, Ni and Ti diffused from the NiTi fiber, and Al, Fe, and Mg diffused from the matrix. The minor elements from both sides could be the major elements at the interface. By selecting the chemical composition of the matrix, it is expected that the chemical composition and crystal structure of the phases formed at the interface can be controlled.

## ACKNOWLEDGMENTS

The authors thank Dr. Samuel Shinizaki for his valuable discussions and his encouragement and Professor Stephanie Brock for her final proofreading on the manuscript and valuable comments. Appreciation is also due to Drs. Xin Wu, Chunlei Xie, and Mohammad Hailat for their early involvement in the fabrication of the NiTi fiber-reinforced Al composites.

## REFERENCES

1. E.T.F. Chau, C.M. Friend, D.M. Allen, J. Hora, and J.R. Webster: *Mater. Sci. Eng. A*, 2006, vol. 438, pp. 589–92.
2. L.H. Yahia, A. Manceur, and P. Chaffraix: *Bio-Med. Mater. Eng.*, 2006, vol. 16 (2), pp. 101–18.
3. R.P. Kusy: *Angle Orthodontist*, 2002, vol. 72 (6), pp. 501–12.
4. J. Abadie, N. Chaillet, and C. LExcellent: *J. Intell. Mater. Sys. Struct.*, 2004, vol. 15 (8), pp. 601–09.
5. W. Huang: *Mater. Des.*, 2002, vol. 23 (1), pp. 11–19.
6. A. Camposeo, F. Fuso, M. Allegrini, E. Arimondo, and A. Tuissi: *Appl. Phys. A*, 2004, vol. 79 (4–6), pp. 1141–43.
7. W.D. Armstrong, T. Lorentzen, P. Brondsted, and P.H. Larsen: *Acta Mater.*, 1998, vol. 46 (10), pp. 3455–66.
8. Y. Furuya: *J. Intell. Mater. Sys. Struct.*, 1996, vol. 7 (5), pp. 321–30.
9. C.A. Rogers: *Smart Materials, Structures, and Mathematical Issues*, Virginia Polytechnic Institute and State University, Blacksburg, VA, 1988, pp. 17–28.
10. C.A. Rogers, C. Liang, and D.K. Barker: *Smart Materials, Structures, and Mathematical Issues*, Virginia Polytechnic Institute and State University, Blacksburg, VA, 1988, pp. 39–62.
11. A. Shimamoto: *Trans. ASME*, 2002, vol. 124 (10), pp. 390–96.
12. G. Murasawa, K. Tohgo, and H. Ishii: *J. Compos. Mater.*, 2004, vol. 38 (5), pp. 399–416.
13. E. Umezaki: *J. Intell. Mater. Sys. Struct.*, 2006, vol. 17 (12), pp. 1115–20.
14. C. Kim: *Int. J. Mod. Phys. B*, 2006, vol. 20 (25–27), pp. 3733–38.
15. Y.J. Zheng, J. Schrooten, and L.S. Cui: *Intermetallics*, 2005, vol. 13 (3–4), pp. 305–08.
16. G.A. Porter, P.K. Liaw, T.N. Tieg, and K.H. Wu: *JOM*, 2000, vol. 52 (10), pp. 52–56.
17. K. Hamada, J.H. Lee, K. Mizuuchi, M. Taya, and K. Inoue: *Metall. Mater. Trans. A*, 1998, vol. 29A, pp. 1127–35.
18. A. Shimamoto, H.T. Zhao, and H. Abe: *Int. J. Fatigue*, 2004, vol. 26, pp. 533–42.
19. C.L. Xie, M. Hailat, X. Wu, G. Newaz, M. Taya, and B. Raju: *J. Eng. Mater. Technol.*, 2007, vol. 129 (1), pp. 69–76.
20. G.A. Porter, P.K. Liaw, T.N. Tieg, and K.H. Wu: *Mater. Sci. Eng. A*, 2001, vol. 314 (1–2), pp. 186–93.
21. G.A. Porter, P.K. Liaw, T.N. Tieg, and K.H. Wu: *Scripta Mater.*, 2000, vol. 43 (12), pp. 1111–17.
22. J.K. Lee: *Compos. Struct.*, 2003, vol. 60, pp. 255–63.
23. K. Mizuuchi, K. Inoue, K. Harnada, M. Sugioka, M. Itami, M. Fukusumi, and M. Kawahara: *Mater. Sci. Eng. A*, 2004, vol. 367, pp. 343–49.
24. P. Stadelmann: *Ultramicroscopy*, 1987, vol. 21, pp. 131–46.
25. *Binary Alloy Phase Diagrams*, Thaddeus B. Massalski, ed., ASM INTERNATIONAL, Metals Park, OH, 1986.
26. P. Villars, A. Prince, and H. Okamoto: *Handbook of Ternary Alloy Phase Diagrams*, ASM INTERNATIONAL, Materials Park, OH, 1995.
27. W.B. Pearson: *A Handbook of Lattice Spacings and Structure of Metals and Alloys*, Pergamon Press, New York, NY, 1958–1967, vol. 1–2.
28. P. Sahu: *Intermetallics*, 2006, vol. 14, pp. 180–88.
29. A.R. Daud and N. Saheb: *Jpn. J. Appl. Phys. Part 2—Lett.*, 2002, vol. 41 (4A), pp. L405–L407.
30. R.E. Watson and M. Weinert: *Phys. Rev. B*, 1998, vol. 58 (10), pp. 5981–88.
31. W. Lin and A.J. Freeman: *Phys. Rev. B*, 1992, vol. 45 (1), pp. 61–69.
32. L.F. Mondolfo: *Aluminum Alloys: Structure and Properties*, Butterworths, London, 1976.
33. *Pearson's Handbook of Crystallographic Data for Intermetallic Phases*, P. Villars and L.D. Calvert, eds., ASM, Metals Park, OH, 1985.
34. P. Budberg and A. Price: in *Ternary Alloys*, G. Petzow and G. Effenberg, eds., VCH, Weinheim, 1992, vol. 5, pp. 309–23.
35. K. Mizuuchi: *JOM*, 2000, vol. 10, pp. 26–31.